Insight into tableted pellets by combining X-ray micro-computed tomography and experimental compaction

Imen Boudina, Eric Rondet, Saeid Nezamabadi, Tahmer Sharkawi

HAL Id: hal-03678035
https://hal.inrae.fr/hal-03678035

Insight into tableted pellets by combining X-ray micro-computed tomography and experimental compaction

Imen Boudina [a,b], Eric Rondet [b], Saeid Nezamabadi [c,d], Tahmer Sharkawi [a,*]

[a] *ICGM, Univ Montpellier, CNRS, ENSCM, Montpellier, France*
[b] *Qualisud, Univ Montpellier, CIRAD, Montpellier SupAgro, Univ d'Avignon, Univ de La Réunion, Montpellier, France*
[c] *LMGC, Univ Montpellier, CNRS, Montpellier, France*
[d] *IATE, Univ Montpellier, CIRAD, INRA, Montpellier SupAgro, Montpellier, France*

ABSTRACT

Pellets are spherical agglomerated particles used to produce multiparticulate pharmaceutical dosage forms. This study aims to develop a new approach that evaluates the deformation behavior of pellets under compression, by combining tableting data and compression models with X-ray micro computed tomography (XMT) image analysis. The deformation of Microcrystalline cellulose (MCC) and sugar pellets known to have different deformation behavior under compression was investigated. Compression data and modeling confirmed the plastic and brittle behavior for MCC and sugar pellets respectively. Image analysis of the XMT showed a different evolution of the morphometric parameters: structure thickness diameter (St Th) and volume equivalent sphere diameter (ESDv). The brittle sugar pellets showed a decrease in both ESDv and St Th parameters while plastic MCC pellets showed a decrease in ST Th and a constant ESDv which is coherent with ductile and brittle material deformation. This study shows that XMT can be used as a tool to characterize the mechanical behavior of pellet particles during compression.

1. Introduction

Pellets are spherical agglomerated particles used to produce multiparticulate pharmaceutical dosage forms. The pelletization process involves the agglomeration of active pharmaceutical ingredients and excipients in spherical units of sizes comprised between 0.5 and 1.5 mm called pellets [1,2]. These multiparticulate systems offer a wide range of therapeutic as well as technological advantages compared with monolithic systems [3]. For example, they disperse as individual units in the gastrointestinal tract thus reducing high local drug concentration (minimizing side effects like the irritation of the gastric mucosa), maximizing drug absorption and reducing plasma concentration fluctuations. Another additional therapeutic advantage is that the drug effect is independent on gastric emptying, thus reducing intra and interindividual variability of the drug plasma concentrations [4,5]. Examples of technological advantages of the pellets are their spherical shape, their narrow particle size distribution and their low friability which ensures very good flow properties necessary for further processing such as coating; capsule filling or tableting [1,2,5,6]. Moreover, these dosage forms allow combining non-compatible drugs or different drug release profiles in the same formulation [7,8].

Pellet compression has received increasing attention over capsule filling because of the many benefits of the tablet dosage form. They are mechanically stronger, can be divided, dispersed into water prior to intake and most importantly, produced at lower cost when compared to capsules. The major challenge during compression of pellets is to anticipate their deformation behavior during this process. Indeed, depending on the mechanical properties of the pellets and the applied stress, compression can either result in an elastic or plastic deformation or even fragmentation of the individual pellets. The understanding of these behaviors is fundamental for the control of the usage properties of tablets generated by pellets compression. The mechanism of deformation of pellets may have a direct impact on the disintegration process and thus on the active pharmaceutical ingredients (APIs) release profile. For example, plastic deformation usually will increase surface contact points between particles, potentially increasing particle cohesion and limiting tablet disintegration [9]. Whereas fragmentation can change pellet functional properties, for example by altering pellet coating integrity or changing drug release profile due to modification in specific surface area. In the same way as for the deformation of native particles, pellets deformation can be described by classical compression models such as Heckel, Kawakita, Walker and Adams models [10,11]. These models are used to describe the global behavior of the powder bulk during compression and also the mean particle mechanical properties [12].

Nevertheless, these models do not provide information on the evolution of individual particle properties during compression such as size, shape, specific surface area variation and their distribution within the compact.

To study the evolution of these morphometric properties during compression, classical granulometric analysis methods (SEM, laser diffraction, sieving, etc.) are not relevant as they require destruction of the tablet to separate the individual particles prior to analysis. The separation process on its own (liquid dispersion/crushing/etc.) can often induce changes in the particle properties thus leading to potential artefacts or false interpretations The use of X-ray micro-computed tomography (XMT), a non-destructive method requiring little sample preparation, is a relevant alternative to determine these particle properties prior to and within the compact after compression. From 2D radiographic projections, XMT provides a three-dimensional image of the inner and outer structure of the sample with a spatial resolution of around one micrometer by measuring the attenuation of X ray beam passing through it at different angular orientations [13]. Following scanning of the object, a backprojection algorithm [14] combines radiographic projections in order to obtain two-dimensional sections of the sample that allow to reconstruct the sample in three dimensions. The final image is composed of voxels having different grey levels corresponding to different density values [15].

XMT literature concerning pharmaceutical tablets and granules focuses mainly on relating density and morphological aspects of the tablets to functional properties. Farber and al., (2003) [16] used XMT to characterize the porosity and morphology of pharmaceutical powder granules. Wu and al., (2008) used XMT to identify the capping problem in pharmaceutical tablets [17]. Sinka and al., (2004) determined material density distributions within pharmaceutical tablets [18]. Finally, Jia and Williams (2006) investigated the structural input for a hybrid mesoscale modeling approach to drug dissolution in tablets [19]. XMT characterization of individual objects size within complex matrices has been previously reported [20,21]. The authors used XMT to determine the bubble size distribution in wheat flour and in non-yeasted wheat flour doughs. Friedrich and al., (2012) [22] showed that XMT can be used to determine the particle size distribution of ideal models made of polydisperse soda glass beads. The aim of their study was to compare the produced distribution with the recommended values for the NIST 1019b standard. They showed that the values of particle sizes measured with XMT were within errors of certified values. In the pharmaceutical field, Fu and al., (2006a, 2006b) [23,24] have extended the application of XMT and image processing to the investigation of a granular system by comparing the XMT particle size distributions with those obtained from SEM picture analysis. Although this study can be considered as an important step, the comparison between size distributions obtained from 2D projection (SEM) and 3D projection (XMT) is problematic. Moreover, no insight on the impact of compression on the evolution in particle size distribution is given. Yang and Fu (2004) [25] have developed a material labeling method using some lead impregnated microcrystalline cellulose particles as an XMT tracer. They managed to characterize particle rearrangement during the early stage of die compaction but no insight about particle size variation was given. Thus, the determination of particle size evolution within tablet during compression using XMT has still yet to be explored.

This study proposes an approach to characterize the mechanical behavior of pelletized materials by combining the use of tableting data, compression models and 3D image analysis generated from XMT in order to evaluate the deformation behavior of pellets under compression. In this study, initial experimental work was performed on an instrumented rotary press simulator by compacting different pelletized materials. Compacts were characterized according to porosity or solid fraction and tensile strength. From the compression data, Heckel, Walker and a recent elasto-plastic model was applied in order to

investigate the behavior of the pelletized material compared to reference pharmaceutical excipients. This initial data is characteristic of the overall particle bed behavior. In order to get individual particle behavior information, this work implemented a complementary tool based on image processing using XMT, to follow the particle size distribution from loose to compacted pellets at different compaction pressures. Two morphometric parameters, Structure Thickness (St Th) and Volume Equivalent Sphere Diameters (ESDv) of pellets were evaluated prior and post compaction.

2. Materials and methods

2.1. Materials

Microcrystalline cellulose (MCC) pellets (MCC PELLETS™ CP-203 SEPPIC, France) and Sugar pellets (Vivapharm Sugar Sphere 40–60 Mesh JRS, France) were used as pelletized materials. These two materials were chosen due to the spherical shape of their particles and the different behavior under pressure (mainly plastic for MCC sphere and mainly brittle for sugar sphere). Microcrystalline cellulose (MCC) (Vivapur 102, JRS Pharma, Germany) and Lactose monohydrate (EXCIPRESS SD2 Armor pharma. France) were used as reference pharmaceutical excipients for the compaction characterization. All powders were sieved between 150 and 300 μm before use.

2.2. Methods

2.2.1. Powder density

True density ($\rho*$) of the excipients was measured in triplicate in a measuring chamber of 35 cm^3 using helium pycnometry (Multi Volume 1305, MICROMERETICS, USA). The true density is 1.51, 1.64, 1.53 and 1.44 g/cm^3 for MCC pellets, sugar pellets, MCC and lactose monohydrate respectively.

2.2.2. Particle characterization

Particle morphology was evaluated by scanning electron microscopy using a Hitachi 4800-S electronic microscope (Hitachi, Tokyo, Japan) at different magnifications. The particle size distribution was determined by dry laser diffraction (Mastersizer 2.18; Malvern Instruments Ltd.). Each measure was performed at least in triplicate and the median particle diameter (d_{50}) was used to express the particle size.

2.2.3. Tableting study

The materials were compressed using an instrumented rotary tablet press simulator (Styl'One Evolution, Medel'Pharm, France). Flat round punches of 11.28 mm diameter were used for the compaction study with a velocity of 15.8 mm.s^{-1} using a default compression cycle adapted for the compaction press simulator used. 400 mg of powder was compacted into tablets at different compaction pressures (from 5 to 300 MPa). Tablet thickness, diameter and crushing strength were measured just after compression using a Sotax Multitester 50FT (Sotax AG, Switzerland). Results were expressed as the mean value of 5 tablets per compaction pressure ± standard deviation. These results were used to calculate:

• The tensile strength (Pa) using the Eq. (1) given below

$$TS = \frac{2F}{\pi dH} \tag{1}$$

where F in N is the crushing strength, d and H are the diameter and thickness of the tablet, respectively, (both in mm) all values read by the Sotax Multitester [26].

• Porosity (n) calculated using Eq. (2) [27,28]

$$n = \left(1 - \frac{\rho^{app}}{\rho*}\right) \times 100 \tag{2}$$

where ρ_{app} and $\rho*$ refer to the apparent density and true density respectively.

• Heckel and Walker modeling

For Heckel modeling [29], three tablets of the different materials, compressed up to 200 MPa, were used. Heckel mean yield pressures (Py) are given by the inverse values of the slope (K) of the following Eq. (3):

$$Ln\left(\frac{1}{n}\right) = KP + A \tag{3}$$

In Eq. (3), n is the porosity and P is the compaction pressure, K is the slope of the linear part of the plot (with the best R^2 fit) and A is the Y axis intercept with the linear part of the Heckel plot. Hersey and Rees (1970) [30] considered that Py values (1/K) can be used to characterize the deformation mechanism of materials. The low value of Py reflects the plastic deformation of a hard-ductile powder while Py high value reflects a fragmentary deformation of a brittle-soft material under compaction force. Very hard ductile materials showed a Py value lower than 40 MPa while very brittle materials have a Py value higher than 200 MPa [31].

For Walker modeling [32], compression data was analyzed according to Eq. (4) to determine decrease in powder relative volume (V) with the increase in the compaction pressure.

$$100V = -Wlog(P) + C \tag{4}$$

Walker modeling uses W (compressibility coefficient) which expresses the percent change in the specific volume of the material when the pressure is increased on log scale, and represents the slop of the line obtained using Eq. (4). The range of pressure used for the linear regression was the same used for Heckel modeling ($R^2 \sim 1$). C is a constant indicating the specific volume at 1 MPa of pressure. Walker modeling is more robust, reproductible and less sensitive to the experimental variations than Heckel modeling [33,34].

• Elasto-plastic modeling

Finally, an elasto-plastic model recently described in literature [35] was applied and compared to the experimental results. The model is based on the relation between the compaction pressure P applied stress and the solid fraction Φ beyond the jamming point according to the following equation:

$$P = \left(1 - f_p\right)\frac{-1}{\frac{1}{M^{eff}} + \frac{1}{cZ\Phi}} \ln \frac{\Phi}{\Phi_j} + f_p P_y \tag{5}$$

where c is a material constant to be determined and adjusted to the model, Z is the coordination number (which, here, being defined as $Z = Z_j + 7.9(\Phi - \Phi_j)^{0.5}$ where Z_j and Φ_j correspond to the jamming point [36]), f_p denotes the ratio between the volume of the plastic regions of particles and their total volume (which, here, being defined as $f_p = \alpha \ln \frac{\Phi}{\Phi_j}$ with α as a constant to be determined), and M^{eff} represents an effective P-wave modulus:

$$M^{eff} = \frac{G^{eff}\left(4G^{eff} - E^{eff}\right)}{3G^{eff} - E^{eff}} \tag{6}$$

Here, E^{eff} and G^{eff} are, respectively, the effective Young's and shear moduli given by:

$$E^{eff} = E\left(1 - \frac{n}{n_c}\right)^{f_E} \tag{7}$$

$$G^{eff} = G\left(1 - \frac{n}{n_c}\right)^{f_G} \tag{8}$$

f_E and f_G denote the characteristic components for Young's and shear moduli, and n_c is the critical porosity, below which the effective Young's and shear moduli become zero. This corresponds to below and near the jamming point. Note that the above relation is defined for elastic-perfectly plastic materials [35].

2.2.4. XMT analysis

Samples of uncompressed and compressed (between 5 and 300 MPa) sugar and MCC pellets were scanned and analyzed to correlate the evolution of morphometric parameters, such as particles granulometry, with the applied stress. Duplicate XMT was performed on uncompressed particles and on the first 2 compacted samples for both Sugar and MCC pellets.

Samples with a known mass were introduced in a polystyrene sample holder. XMT imaging was carried out with a Bruker SkyScan 1272 high resolution scanner. The samples were scanned at a nominal resolution of 4 μm. The current (U, eV), the intensity (I, μA) of the X-ray beam as well as the nature and thickness of filters vary according to the sample (nature of particles and sample density variation) and were selected to obtain a constant signal transmission of 30%. The X-Ray power source (P=U·I) is kept constant at 10 W. A camera pixel binning of 4032 × 2688 was applied. The scanned orbit was 180 degrees with a rotation step of 0.2° adapted to the magnification.

Bruker's NRecon® software was used to reconstruct the scan projections into 2D images using Feldkamp algorithm [14]. Gaussian smoothing, ring artifact reduction and beam hardening corrections were applied.

Volume rendered 3D images (Fig. 1) were generated using an RGBA transfer function in SkyScan CTVox® software.

Image analysis was performed using SkyScan CTAn® software. A specific task list analysis described below was developed to individualize particles within the pellet bed or the pellet compacts so as to evaluate the change in particle size distribution according to the increase in compression stress.

Two image segmentations were successively carried out on the original image (Fig. 2a): the first one to define the sample volume of interest (VOI) and the second one to define the object volume (powder particles volume) within this VOI (Fig. 2b). To avoid subjective segmentation, a grey level threshold was set by successive iterations in a way to fall in a volume object (V) equal to:

$$V = \frac{m}{\rho*} \tag{9}$$

where m is the mass of the object (the entire sample i.e. all loose or compacted pellets) subjected to acquisition and $\rho*$ is the true density of the material as measured by a helium pycnometer.

After image binarization, a 3D watershed separation was used to dissociate particles that appeared joined together (Fig. 2c).

Each stage of the image analysis task list (filtering with a median filter and tolerance value for watershed separation) was chosen to have the closest d_{50} values between XMT and laser diffraction granulometry. As shown in Fig. 3, the particle size distribution obtained with XMT gives narrower populations compared to laser diffraction method. The XMT distributions detect few or no particles larger than 300 μm, unlike the laser diffraction method. Since the particles were all sieved between 150 μm and 300 μm, this difference is explained by the physical artifact associated to laser diffraction previously mentioned in other studies
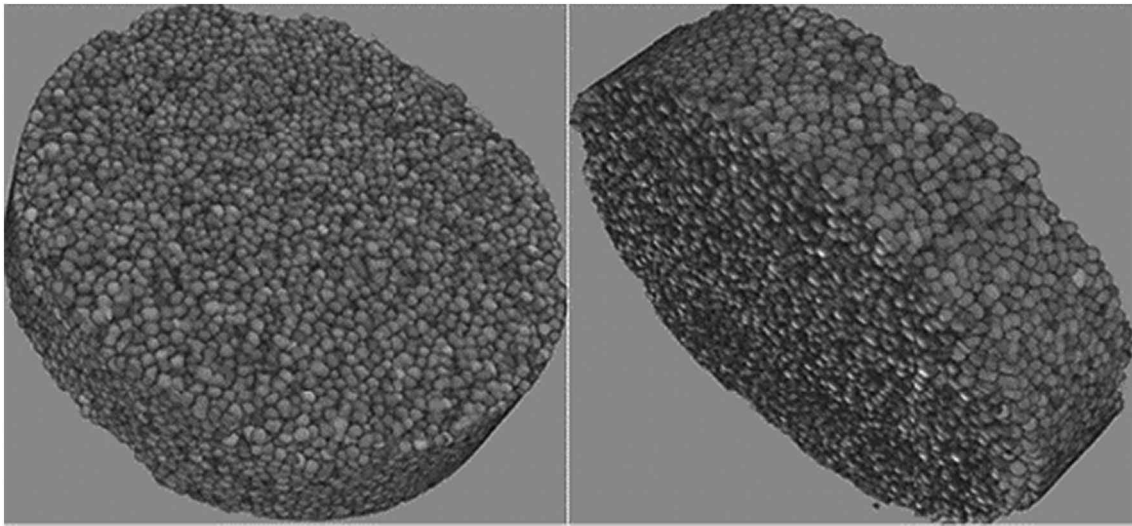
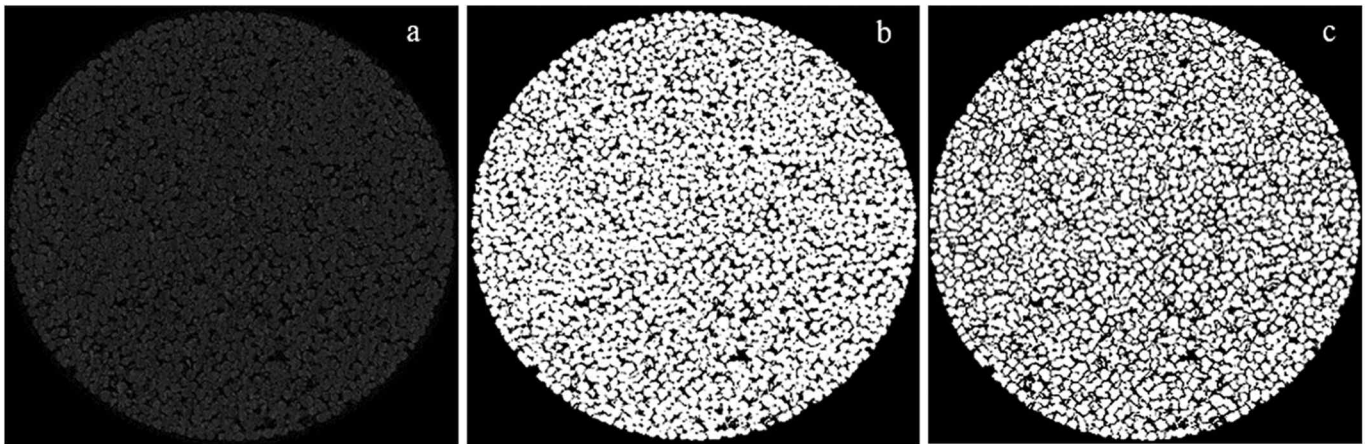**Fig. 1.** 3D image of a 11 mm diameter Tablet of MCC pellets visualized in CTvox software.

Fig. 2. Analysis steps starting from the original image (a), binarized image before watershed separation (b), binarized image after watershed separation (c).
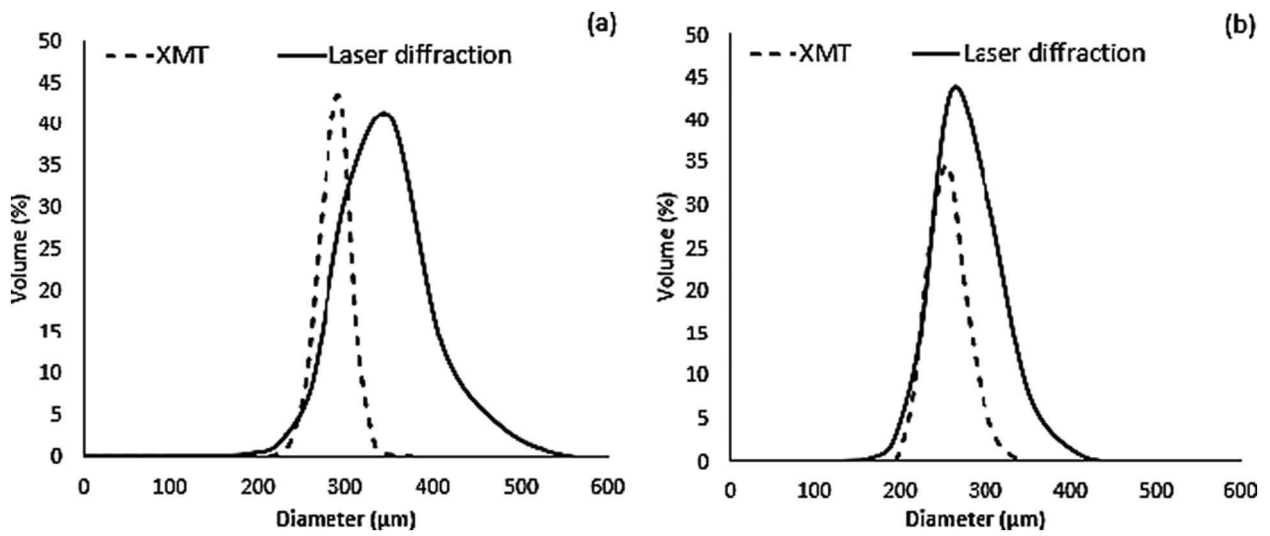

Fig. 3. Comparison between XMT and laser diffraction particle size distributions: MCC pellets (a) and sugar pellets (b).
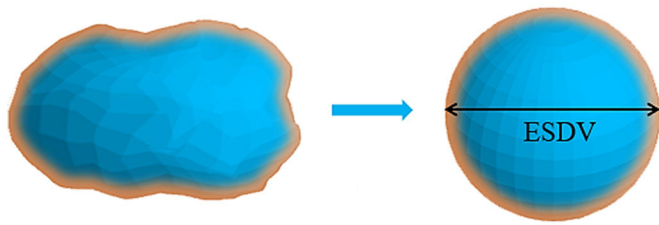
Fig. 4. Schematical representation of the ESDv of a non-spherical particle.

[37–40] and by the fact that the measurement of the particle size of non-perfectly spherical shapes takes into account the projected cross section averaged over all the particle's possible orientations relative to the direction of the beam. This overestimates the size of less spherical particles [41]. Equally, with nominal resolution of 4 μm., a 300 μm pellet

has a digital size of 75 pixels acros. If one considers an uncertainty of 2 pixels at each end, this can represent an uncertainty of approximately 5% of the pellet size.

Two morphometric parameters were selected to follow the evolution of the particle size distribution during compression: Structure thickness (St Th) and Volume Equivalent Sphere Diameters (ESDv). ESDv is the diameter of the sphere that would have the same volume as the discrete 3D object (Fig. 4). It is estimated by the following formula: $ESDv = \sqrt[3]{(6V_p/\pi)}$ where V_p is the particle volume. St Th is the diameter of the largest sphere which can be fitted completely inside the particle as shown in Fig. 5. The calculation of the St Th is preceded by a skeletization in which the two medial axes are identified. Then the "sphere-fitting" local thickness measurement is made for all the voxels lying along this axis.

ESDv and St Th are calculated from the 3D images for all individual binarized 3D objects within the VOI. A specific code was created with R studio® software to obtain sample granulometric distributions.
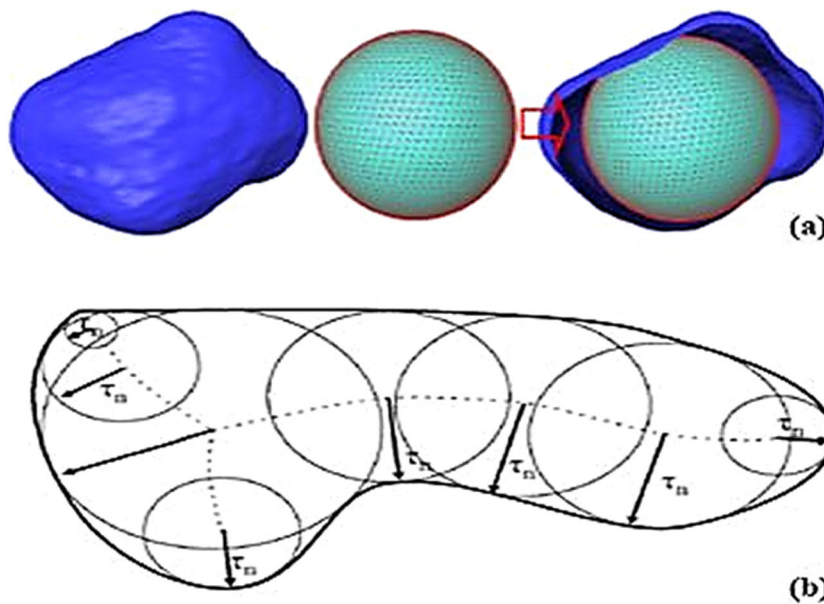

Fig. 5. 3D example of the largest sphere which can be fitted within a particle (a). Schematic representation of the determination of the structure thickness starting with the skeletonization (b) [43,44].
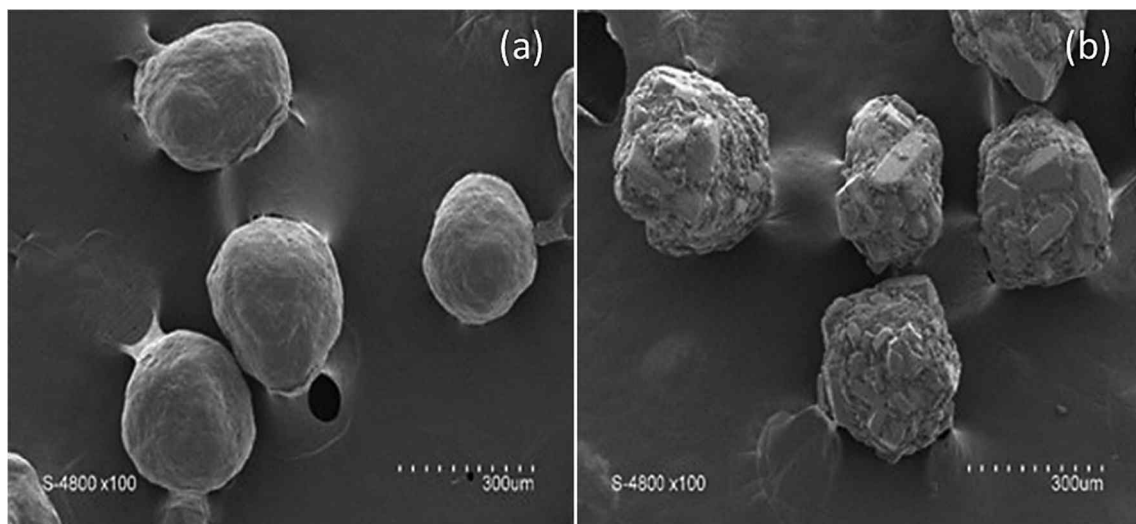

Fig. 6. Scanning electron microscopy of uncompressed MCC (a) and sugar (b) pellets.

Several granulometric deciles (d_{10}, d_{50}, d_{90}) were calculated from the resulting distributions. Granulometric distribution span (($(d_{90} - d_{10})/d_{50}$) was calculated on each distribution.

3. Results and discussion

3.1. Morphology, tabletability and compressibility

Fig. 6 shows SEM acquisitions of MCC and Sugar pellets. MCC pellets have homogeneous, smooth and regular surfaces. This surface aspect is typical of the extrusion-spheronization process used to produce the pellets [2]. Sugar pellets are more irregular and show agglomerated smaller particles that are visible on the surface of the pellets. Particle size by laser diffraction (Fig. 3) shows median particle size of 215 μm for MCC pellets and 310 μm for the sugar pellets. The particle morphology, size range and distribution are properties that have an effect in the rearrangement phase and thus on the overall compaction behavior, therefore we aimed to minimize these variables by selecting relatively spheroidal shaped particles and by sieving them prior to use.

As shown in Fig. 7a, tablets from pellet material show lower tensile strength value than the tablets from the non-pelletized lactose and MCC reference materials. Non pelletized MCC is a reference pharmaceutical tablet filer that is known to show strong tablet cohesiveness upon compaction resulting from the increased surface contact points of the MCC particles and its high ability to form hydrogen bonding at these contact points [31,44–46].

The pelletized MCC on the other hand shows the lowest tensile strength value with very little evolution upon increasing compaction pressures. The reduced tabletability performance of the pelletized MCC is explained in literature by the decrease of the inter-particle hydrogen bonding [31,47–49]. As these pellets have a smoother surface and higher sphericity than non-pelletized MCC particles there are fewer contact points between particles resulting in lower cohesion values. Furthermore, it is reported that the loss in the bonding capacities between particles is also explained by the fact that the extrusion-spheronization process to produce these pellets creates strong intra pellet hydrogen bonding of the native MCC particles which in turn limits the inter-particle interaction within the compacted pellets [31,50]. This is shown by a significant drop in cohesion forces when compared to non-pelletized MCC particles. Pelletized sugar and lactose have
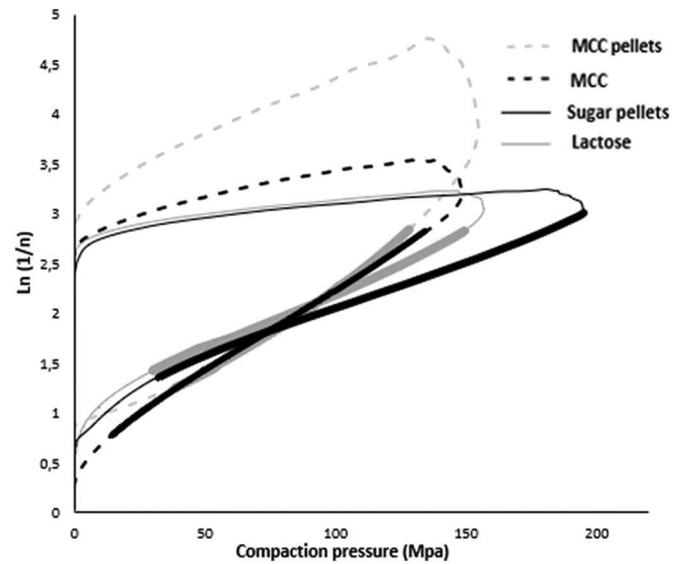

Fig. 8. Heckel profiles of pellets and reference materials.

similar tabletability profiles at the lower compaction pressure while lactose tablets have increased tensile strength at the higher compaction pressures. This again can be explained from the decrease in contact points for the pelletized sugar particles compared to non-pelletized lactose that decreases cohesiveness.

Fig. 7b shows the compressibility profiles of the pelletized and reference materials. Here pelletized materials are less compressible than non-pelletized materials. This again is attributed to the high sphericity of the pelletized materials and to the tighter size distribution (lower span value) of the pelletized materials compared to the non-pelletized reference materials: 0.4; 0.43; 0.71 and 0.73 for sugar pellets, MCC pellets, Lactose and MCC respectively. The pelletized powders are thus less prone to rearrangement and packing capabilities than more irregular particle morphologies. The results also show that despite less cohesiveness than sugar pellet tablets, the MCC pellets are more compressible. These results are explained by the highly plastic deformation nature of MCC compared to sugar.
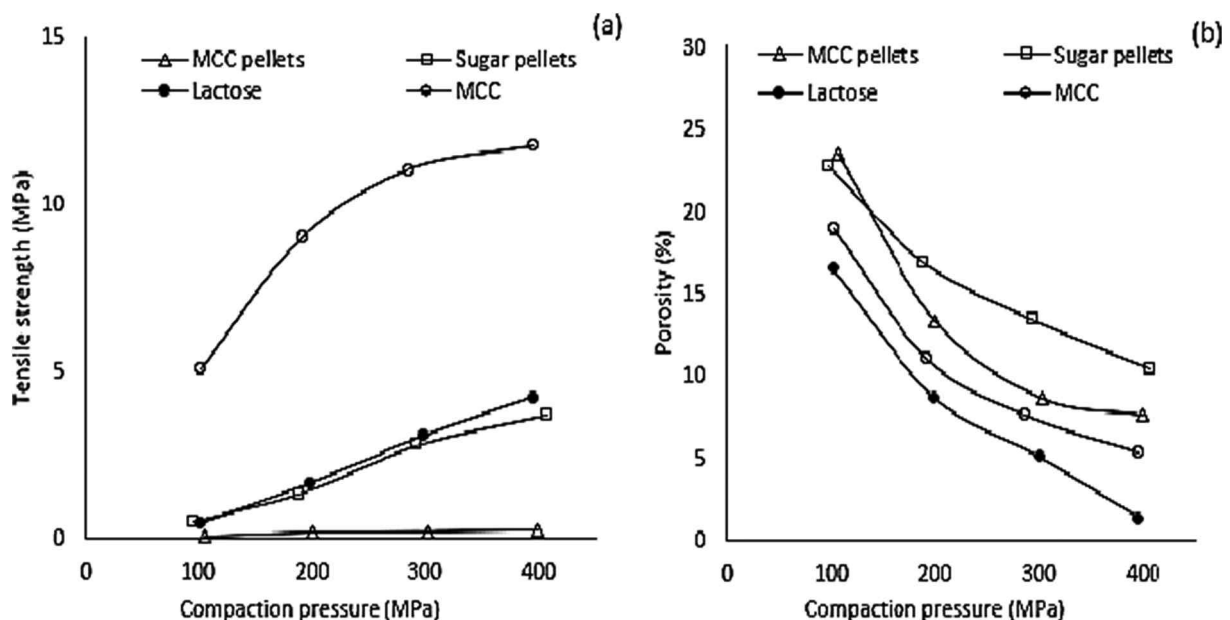

Fig. 7. Tensile strength (a) and porosity (b) as a function of compaction pressure of pellets and reference materials.

Table 1
Mean yield pressure values and compressibility index.

	P range[*] (MPa)	Py (MPa)	W	Classification
MCC pellets	38–128	58.5	64.8	Plastic
Sugar pellets	33–192	103.1	37.7	Brittle
MCC	15–134	59.5	81.6	Plastic
Lactose	31–153	87.79	38.4	Brittle

[*] P range is the range of the pressure used to calculate the Py and W.

3.2. Heckel, Walker and elasto-plastic modeling

Deformation behavior was modeled by Heckel [29], Walker [32] and elasto-plastic [35] equations. Heckel parameter (Py) was used as an approximate indicator to compare pellet deformation behavior [51–53]. In literature [54–58], MCC is considered as ductile material that undergoes plastic deformation whereas lactose is more of a brittle material that undergoes fragmentation. According to Hooper and *al.*, (2016) [59], for a Py value ˜80 MPa, the material is considered as ductile and undergoes plastic deformation while a value of Py > 80 MPa indicates a brittle material that undergoes fragmentation.

Fig. 8 shows the evolution of the in-die Heckel plots. The true density and the compact thickness calculated from the corrected punch displacement were used to determine the porosity (n).

According to Table 1, non pelletized and pelletized MCC particles have very similar Py values of 59.5 MPa and 58.5 MPa respectively. These values are in agreement with literature of plastically deformed materials [34,60]. This shows that despite the difference in properties in terms of cohesiveness, the pelletization does not change the deformation mode according to Heckel modeling. The plastic deformation

of the MCC pellets after compaction can be observed also in the SEM images of Fig. 9. These images show particles that were manually recovered after compaction from the compacts. They show how the sphericity of the MCC pellets is gradually changed to polyhedral particles as the compaction pressure increases without any signs of particle fragmentation. Table 1 shows that sugar pellets and Lactose have a Py values that are higher compared to MCC and are more reflective of brittle materials as reported by literature [55,56,58,61]. This fragmentation of the sugar pellets when compaction stress increases is also shown by the SEM pictures (Fig. 10) of recovered particles after different compaction pressures.

For the Walker modeling (Fig. 11), reference materials have given distinct values of W; MCC considered as plastic material presented the highest value (81.6) while lactose (brittle material) showed a low value (38.4). Literature reports a material is considered to be more plastic when it possesses the highest value of W [31,62]. The W value of the sugar spheres (37.7) is close to that of lactose and highlights the fact that it behaves as a brittle material that undergoes a fragmentary deformation mechanism under compaction pressure. On the contrary, MCC pellets' W value is higher (64.8) and close to that of MCC which reveals a more plastic deformation behavior.

Finally, the elasto-plastic model (Eq. (5)) is applied to the experimental results. The elasto-plastic model uses mechanical properties of the material that composes the individual particles (Young's and Shear's moduli) and is a complement to the traditional Heckle Walker modeling that are based on empirical phenomenological observation of powder bed volume reduction. This is a recent model developed in the context of numerical simulations and strictly applying to after the jamming point of particles. Since this paper introduces XMT as a tool to characterize individual particle behavior we used this new model to confirm our
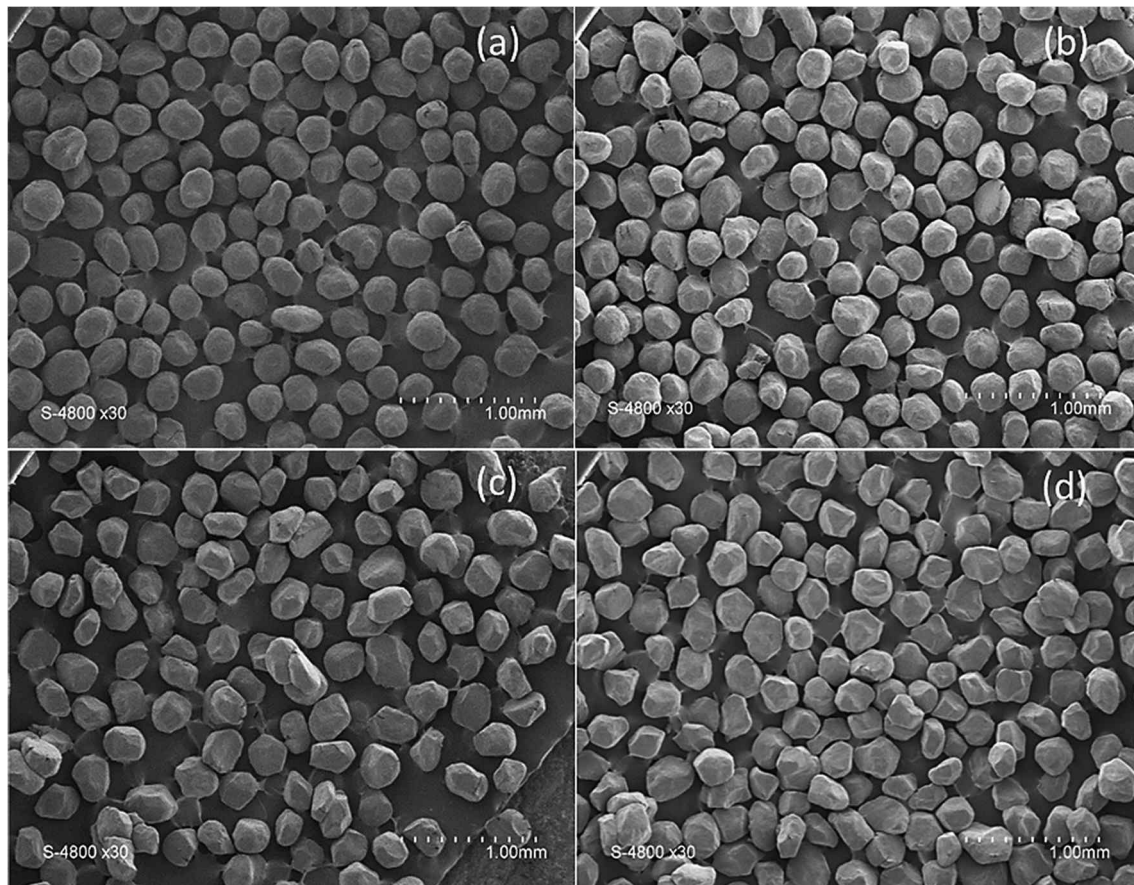

Fig. 9. MCC compacted pellets retrieved after a compaction pressure of: 50 MPa (a), 100 MPa (b), 200 MPa (c) and 300 MPa (d).
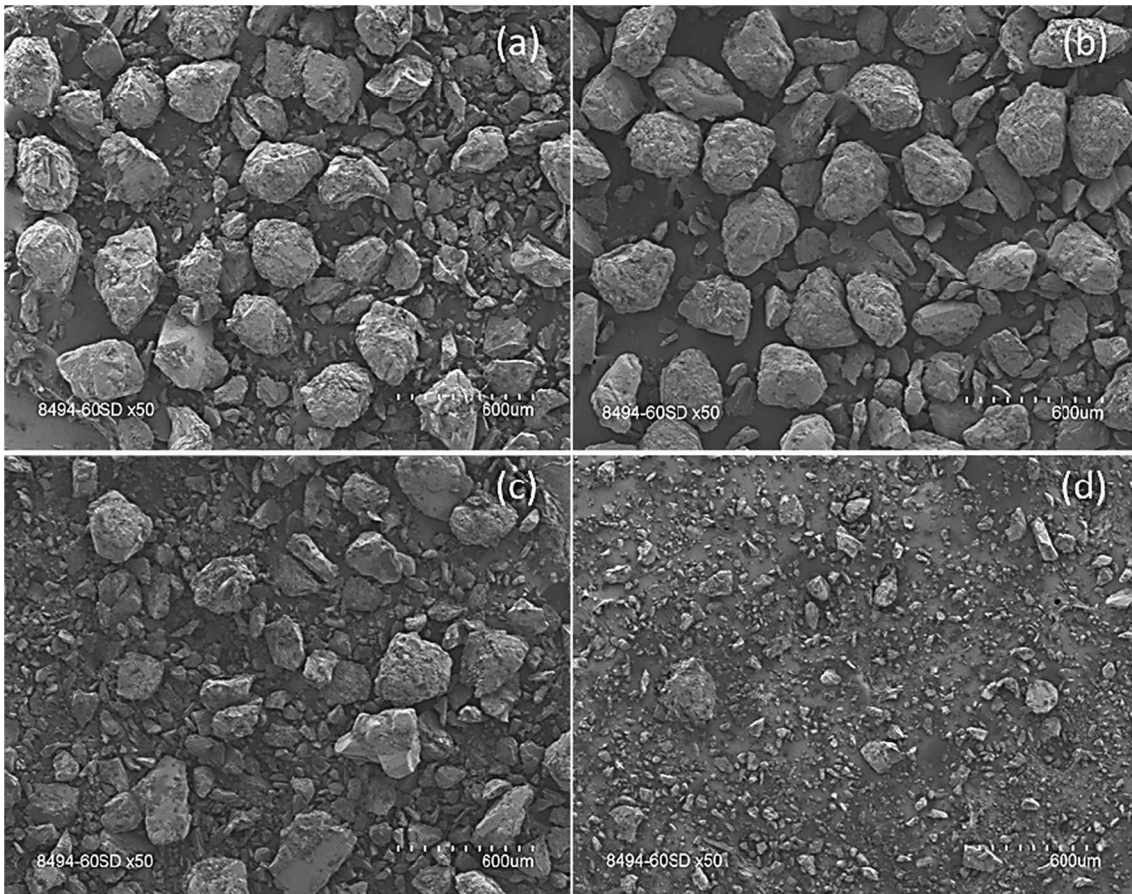
Fig. 10. Sugar compacted pellets retrieved after a compaction pressure of:: 5 MPa (a), 15 MPa (b), 25 MPa (c) and 50 MPa (d).
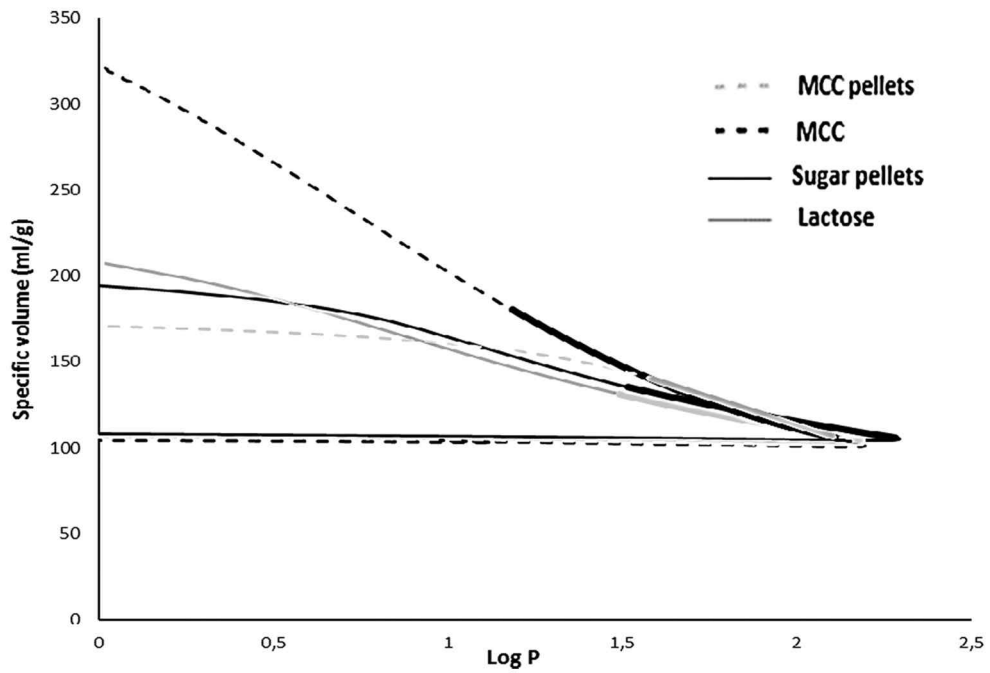

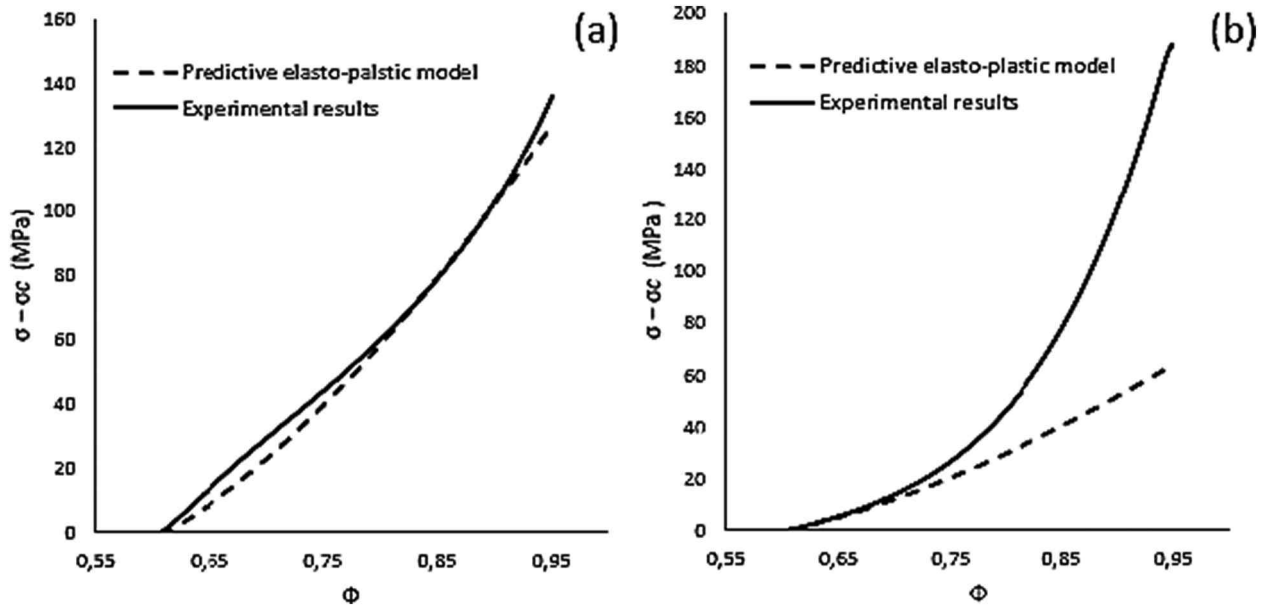**Fig. 11.** Walker profiles of pellets and reference materials.

Fig. 12. Applied stress $\sigma - \sigma c$ as a function of packing fraction Φ of MCC pellets (a) and Sugar pellets (b).

experimental results of individual particle, which is not possible with the traditional empirical models.

We consider, here, $Z_j = 6$ and $\Phi_j \approx 0.6$ [37]. We also set $f_E = f_G = 1$ and $n_c = 0.4$ ($\approx 1 - \Phi_j$) for the two materials. Fig. 12 shows the predictions of the elasto-plastic model for the MCC pellet ($c = 29$ MPa and $\alpha = 0.02$) and the Sugar pellet ($c = 14$ MPa and $\alpha = 0$) as well as the experimental data. For the plastically deforming MCC, the prediction of the model is in good agreement with the experimental values over most of the solid fraction range with a slight divergence at the very high solid fraction values. For the Sugar pellets on the other hand, there is a divergence quite early showing that the elasto-plastic behavior is not respected anymore and that one can consider that above the further reduction in solid fraction can be mainly attributed to fragmentation. These results are again in agreement with the previous modeling.

3.3. XMT evaluation of morphometric and granulometric parameters within compacts

The aim of this section is to demonstrate the ability of the tomographic tool to quantify the deformation and fragmentation of particles that have undergone uniaxial stress during compaction to produce a tablet. Sugar pellets and MCC pellets tablets are generated from native pellets using compression of increasing pressure. Morphometric parameters ESDv and St Th are measured on each particle constituting the compact. The relevance of these measurements depends on the ability of the optimized image processing algorithms used, and particularly the Watershed Separation step, to be sufficiently efficient to individualize all particles within the compact, whatever the compaction stress. Fig. 13, show a tablet produced after tomographic analysis of sugar pellets compacts, highlights the fact that the majority of the particles within the compact can be separated from each other, thus allowing their morphometric evaluation. However, it is also possible to visualize (in white) elements with ESDv that are bigger than the initially sieved particles (between 150 and 300 μm). These elements are the result of the particles merging in such a way that the watershed separation algorithm becomes unable to separate them thus defining particles that are bigger than the initial uncompressed particles. Table 2 and 3 show particle populations that are higher than the upper 300 μm limit by sieving. The number of these elements that are mainly located in the peripheral

areas of the compact where the intensity of compaction stress is highest due to the die walls and thus increases with the applied pressure. As it will be discussed later, the size distributions of the ESDv should thus exhibit a slight increase in size. This increase cannot be physically explained by an effect of compression and is the result of the limitation in the watershed separation image analysis tool as shown in Tables 2 and 3 by particles that are bigger than the upper 300 μm limit by sieving.

3.3.1. Structure thickness diameter (St Th)

Fig. 14 shows the evolution of structure thickness distribution for MCC pellets (a) and Sugar pellets (b) according to compression stress. The granulometric deciles values are shown in Table 2. The evolution for MCC pellets St Th with compression shows a reduction in median size (16% between 0 and 300 MPa) as well as a reduction in span (47% between 0 and 300 MPa). As a result of the applied stress on all the particles, their St Th decreases almost homogeneously, causing a shift to smaller size distributions. Concerning sugar pellets, the increase in compaction pressure induces a drop in the median size (%) but an increase in span of the size distribution (124%). Between 0 and 100 MPa, the clear decrease in d_{10} (56%) compared to that of d_{90} (34%) shows that the stress is applied inhomogeneously within the medium, leading to the fragmentation of some elements while others remain unchanged in size. The overall size reduction of particles within the bulk is the result of the progressive production of a population of small particles resulting from a fragmentation process to the detriment of the larger ones.

3.3.2. Volume equivalent sphere diameter (ESDv)

Fig. 15 shows the evolution of the volume equivalent sphere diameter (ESDv) distribution as a function of compaction pressure for MCC pellets (b) and Sugar pellets (b). In both materials, one part of the ESDv fraction increases when the compaction pressure rises. As explained earlier in this section, and since it is not possible for individual particles to increase in size during compression, the explanation lies in the merging of particles during compaction that the XMT image processing (Watershed Separation) is not able to individualize any more. This can be quantified by the granulometric deciles values above the 300 um shown in Table 3 for the highest compaction pressures.

Fig. 16 shows that particles of MCC pellets with an ESDv higher than 300 μm results from the merging of individual particles. This merging
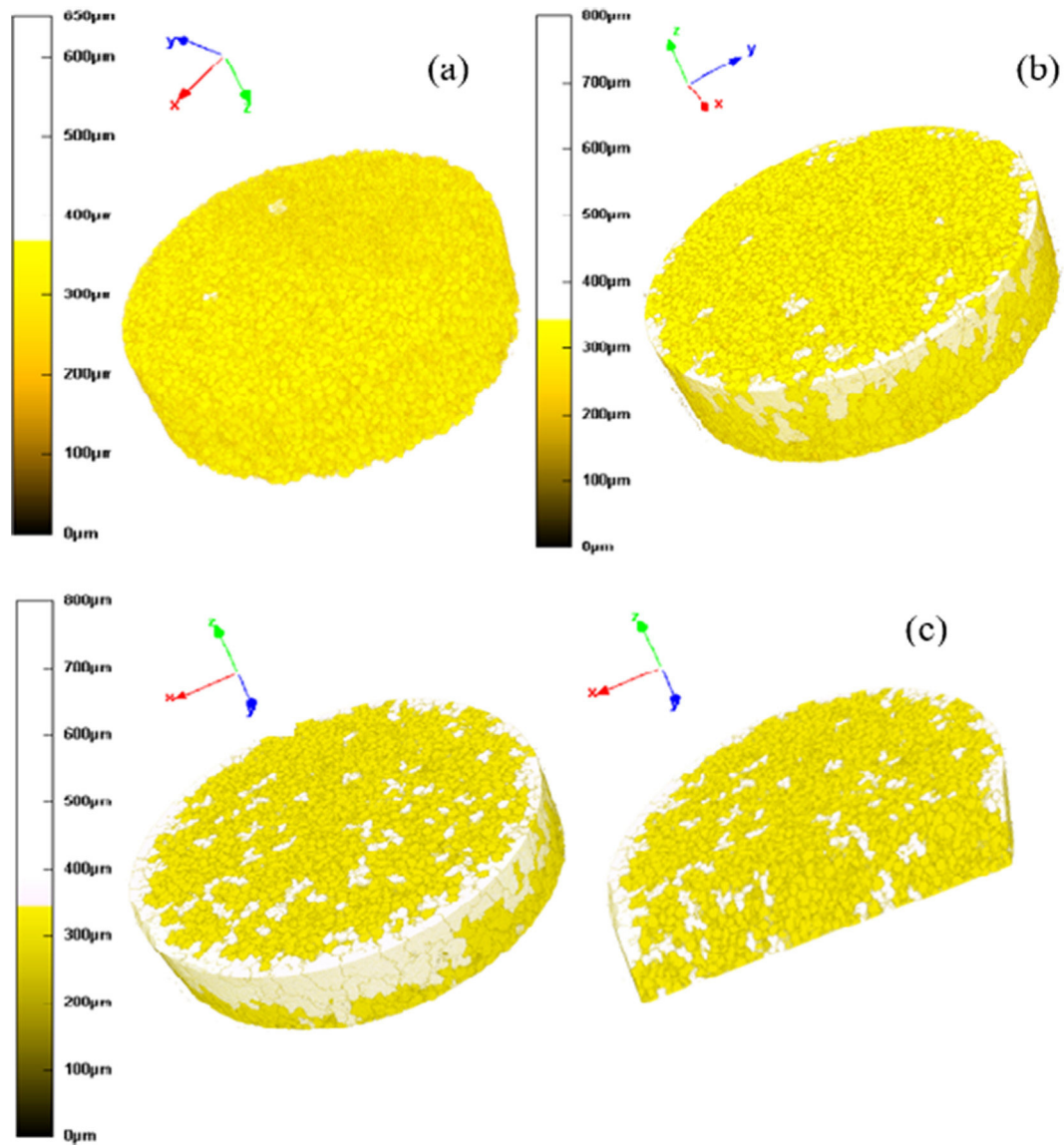
Fig. 13. 3D image of a 11 mm diameter tablets of sugar pellets compacted at 25 MPa (a), 50 MPa (b) and 100 MPa (c).

Table 2
d_{10}, d_{50}, d_{90} and span of the Structure Thickness diameter of MCC and Sugar pellets at different compaction pressures.

P (MPa)	d10 (μm)	d50(μm)	d90(μm)	Span
0	147 ± 1	188 ± 3	223 ± 2	0.40 ± 0.01
50	132 ± 4	167 ± 4	202 ± 3	0.43 ± 0.01
100	131 ± 1	160 ± 2	185 ± 5	0.34 ± 0.03
200	130	154	178	0.31
300	140	158	175	0.21
0	160 ± 0	196 ± 0	224 ± 1	0.33 ± 0.01
5	127 ± 10	178 ± 12	215 ± 10	0.50 ± 0.04
10	100 ± 3	155 ± 4	203 ± 4	0.67 ± 0.01
15	74	107	157	0.78
25	72	105	153	0.78
50	66	101	148	0.82
100	71	105	148	0.74

Table 3
Evolution of d_{10}, d_{50}, d_{90} and span of ESDv diameters of MCC and Sugar pellets at different compaction pressures.

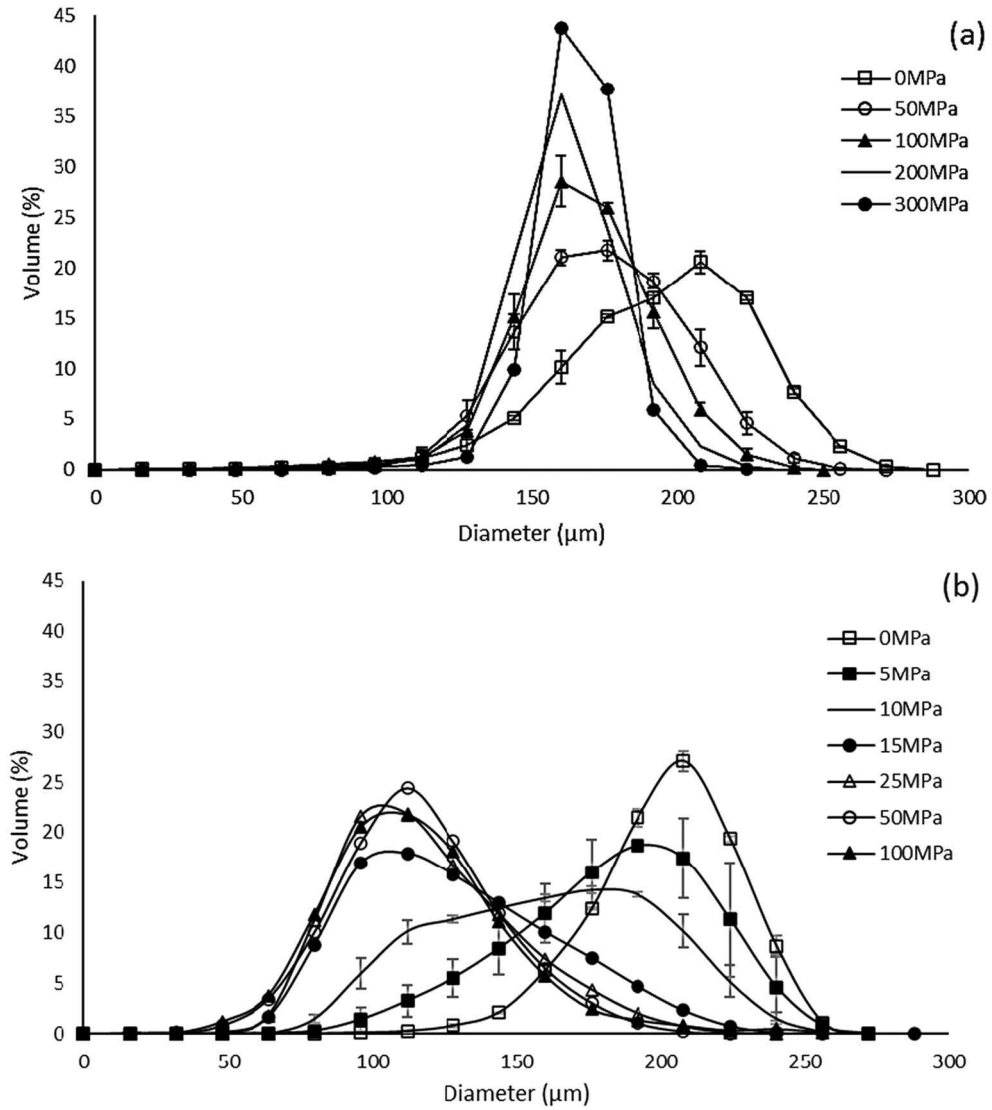| P (MPa)	d10(μm)	d50(μm)	d90(μm)	Span
0	216 ± 2	245 ± 3	279 ± 5	0.26 ± 0.01
50	217 ± 0	251 ± 0	308 ± 0	0.36 ± 0.01
100	222 ± 1	272 ± 1	351 ± 2	0.47 ± 0.01
200	226	287	371	0.51
300	255	361	496	0.67
0	253 ± 2	279 ± 2	304 ± 3	0.18 ± 0.00
5	249 ± 3	280 ± 3	308 ± 3	0.21 ± 0.00
10	243 ± 3	284 ± 3	326 ± 5	0.29 ± 0.01
15	245	292	354	0.37
25	249	309	382	0.43
50	219	289	350.3	0.45
100	243	311	402	0.51

Fig. 14. Structure thickness diameter distribution at different compaction pressures for MCC pellets (a) and sugar pellets (b).
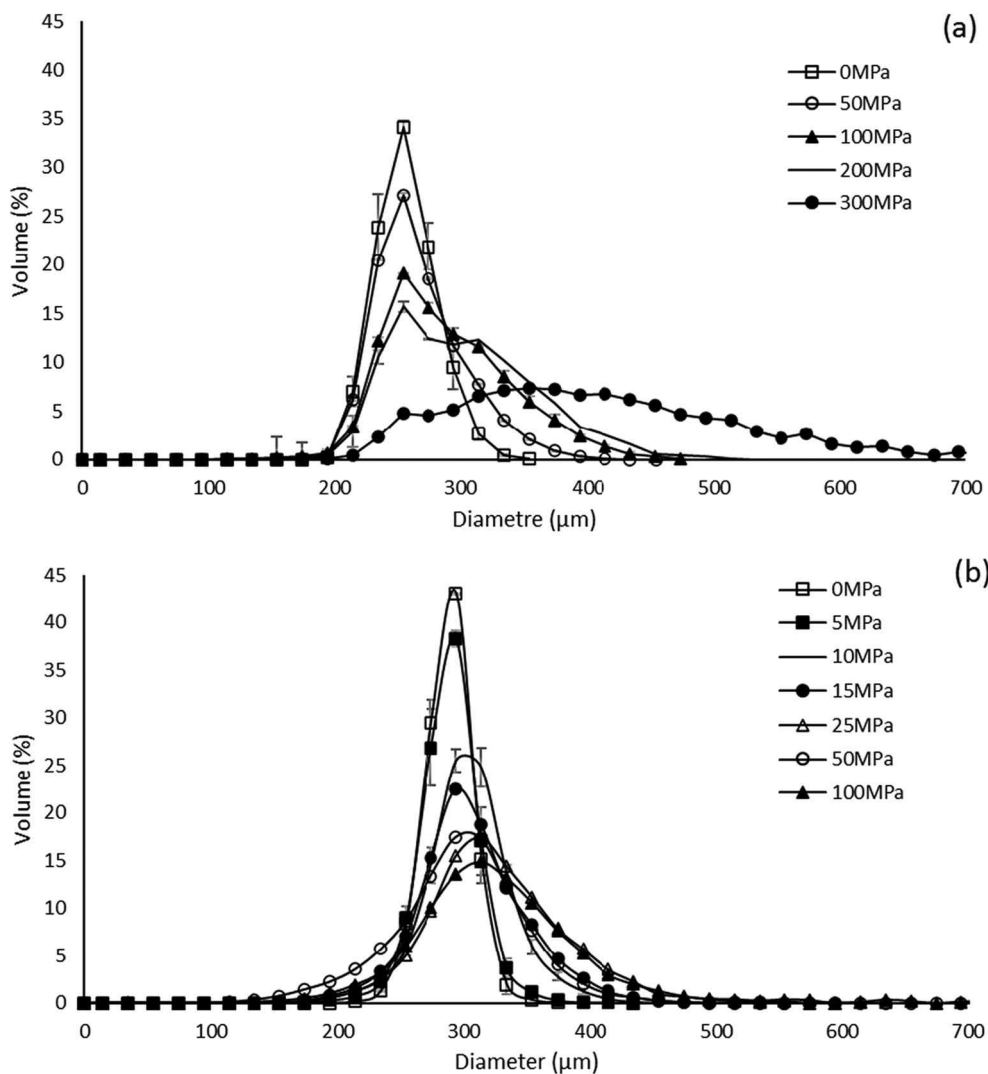
Fig. 15. Volume equivalent sphere diameter with compaction pressure for MCC pellets (a) and sugar pellets (b).

increases as the compaction pressure rises and more contact points and merging of surface area appear. For the Sugar pellets, Fig. 15 makes it is possible to highlight the gradual appearance of small particles resulting from the fragmentation of bigger ones when compaction pressure increases. This phenomenon can be highlighted by the decrease of 13% in the d_{10} value of sugar sphere ESDv between 0 and 50 MPa. Concerning MCC pellets, the appearance of such a small size fraction is absent from the ESDv size distribution which is coherent with a plastic deformation.

These results concerning both the evolution of St Th and ESDv according to compaction pressure make it possible to quantitatively differentiate plastic deformation from fragmentary behavior during compaction. As shown in Fig. 17, the change in structure thickness diameter of a plastic or fragmentary material is different. Upon compression, plastic material deform so that their St Th decreases but their volume remains constant. ESDv of plastic particles thus remains constant during compression. When considering brittle material, compaction induces fragmentation of some particles which translates into a decrease of both St Th and ESDV (due to a decrease in the volume of the particle). Thus, following the change of these two morphometric parameters during compaction makes it possible to distinguish between the materials with opposite behavior (plastic vs brittle). It is mentioned that due to the long calculation time (over 4 h) and the pixel limited

resolution of acquisition, XMT is not meant to be used as an analytical tool to express exact particle size and particle size distribution but as an indicator of the size and distribution evolution.

4. Conclusion

The objective of this study was to develop a methodology combining X-ray micro-computed tomography and experimental compaction to evaluate pellet deformation behavior under stress. The approach of uniaxial solicitation of the particles constituting the medium to determine the mechanical properties (Young's modulus, breaking point…) is not effective because it requires reproducing the test on a very important number of particles to obtain representative data. Thus, traditionally, the deformation behavior of materials undergoing compaction is evaluated on overall particle bed behavior scale by reduction of the bed volume according to compaction pressure. The modeling of the evolution of the powder bed volume properties as a function of the applied stress, makes it possible to determine parameters that distinguish between materials undergoing brittle failures or showing a ductile behavior. The tomographic acquisitions and the image processing that followed the compression showed a different evolution of the morphometric parameters (ESDv and St Th) which are able to quantify particle size evolution and explain particle deformation and fragmentation behavior.
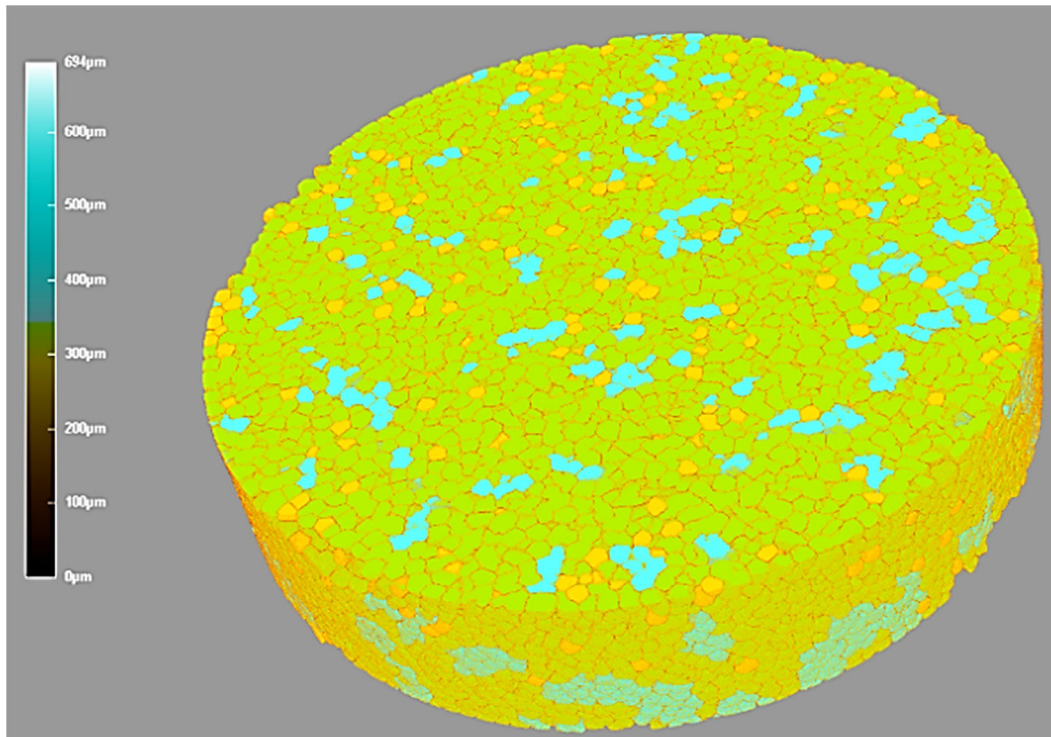
Fig. 16. Particle merging phenomenon in 11 mm diameter tablets of MCC pellets at 300 MPa.

A plastic material will show a St Th decrease while the ESDv remains constant during compression. A fragmenting brittle material will show a decrease in both parameters (St Th and ESDv). These behaviors were confirmed by three different modeling equations of the experimental compression profiles thus validating the morphometric parameters. Additionally, by using material specific properties (Young's and Shear moduli) the elasto-plastic provides insight on the particle deformation behavior that can be related to individual particle deformation. This
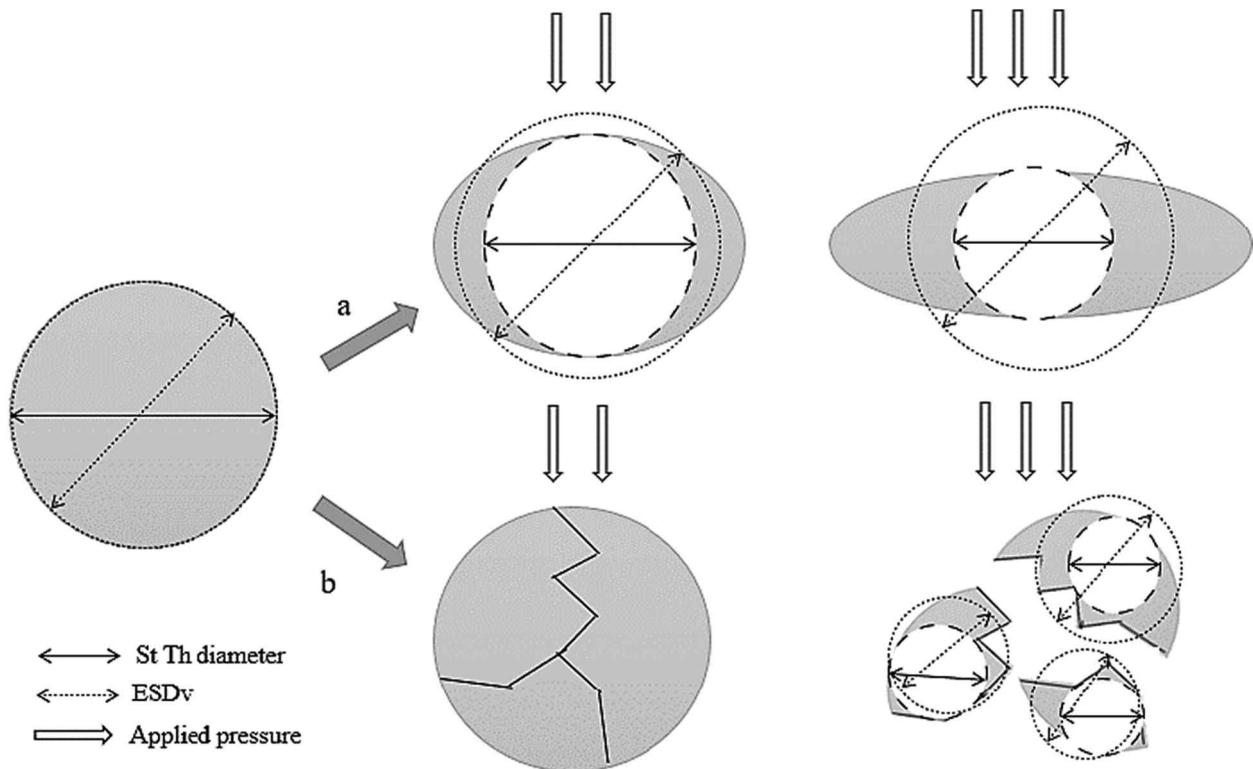

Fig. 17. 2D representation of the change of the St Th and ESDv diameter under pressure in ductile material (a) and brittle material (b).

work describes an original approach in which XMT can be used as a tool to evaluate particle behavior under compression. Although there are some limitations regarding the image analysis algorithm used (watershed separation and pixel resolution),this work lays the ground for deeper understanding of individual particles undergoing compression within a particle bed. XMT can provide more detailed information on the individual particle shape modifications as well as localized deformation within the compact. This promising methodology can be used in future work to help chose the formulation strategies for pharmaceutical tablet compacts, as it allows to explain how material deformation mechanism takes place during the compaction process and to formulate with specifically chosen excipients to accommodate active ingredients or specific tablet properties.

Declaration of Competing Interest

The authors declare that they have no known competing financial interests or personal relationships that could have appeared to influence the work reported in this paper.

Acknowledgements

References

[1] N. Yadav, A. Verma, Pharmaceutical pellets: a versatile carrier for oral controlled delivery of drugs, Indian J. Pharm. Educ. 50 (2016) S146–S160.

[2] T.T.L. Nguyen, Extrusion-Spheronization of Pharmaceutical Products: System for the Delivery of Active Ingredients which are Poorly Soluble by Oral Route, université de Strasbourg, 2017.

[3] M.E.M. Teran, Development and Evaluation of Controlled Release Pellets in Orodispersible Tablets for Pediatric Use, Université du Droit et de la Santé-Lille II., 2016

[4] R. Bodmeier, Tableting of coated pellets, Eur. J. Pharm. Biopharm. 43 (1) (1997) 1–8.

[5] N. Jawahar, P.H. Anilbhai, Multi unit particulates systems (MUPS): a novel pellets for oral dosage forms, J. Pharm. Sci. Res. 4 (9) (2012) 1915.

[6] E. Gryczová, K. Kubova Dvorackova, M. Rabiškova, Evaluation of pellet friability, Ceska Slov. Farm. 58 (2009) 9–13.

[7] J. Pinto, M. Lameiro, P. Martins, Investigation on the co-extrudability and spheronization properties of wet masses, Int. J. Pharm. 227 (1–2) (2001) 71–80.

[8] U. Quintavalle, et al., Preparation of sustained release co-extrudates by hot-melt extrusion and mathematical modelling of in vitro/in vivo drug release profiles, Eur. J. Pharm. Sci. 33 (3) (2008) 282–293.

[9] D. Markl, J.A. Zeitler, A review of disintegration mechanisms and measurement techniques, Pharm. Res. 34 (5) (2017) 890–917.

[10] V. Khot, et al., Optimisation of granulation techniques for development of tablet dosage form, Indo Am. J. Pharm. Sci. 4 (12) (2017) 4626–4639.

[11] J. Nordström, et al., On the physical interpretation of the Kawakita and Adams parameters derived from confined compression of granular solids, Powder Technol. 182 (2008) 424–435.

[12] E. Rondet, T. Ruiz, B. Cuq, Rheological and mechanical characterization of wet agglomerates processed in low shear mixer, J. Food Eng. 117 (1) (2013) 67–73.

[13] E.N. Landis, D.T. Keane, X-ray microtomography, Mater. Charact. 61 (12) (2010) 1305–1316.

[14] L.A. Feldkamp, L.C. Davis, J.W. Kress, Practical cone-beam algorithm, J. Opt. Soc. Am. A 1 (6) (1984) 612–619.

[15] P.J. Withers, et al., X-ray computed tomography, Nature Rev. Methods Primers 1 (1) (2021) 18.

[16] L. Farber, G. Tardos, J.N. Michaels, Use of X-ray tomography to study the porosity and morphology of granules, Powder Technol. 132 (1) (2003) 57–63.

[17] C.Y. Wu, et al., Numerical and experimental investigation of capping mechanisms during pharmaceutical tablet compaction, Powder Technol. 181 (2) (2008) 121–129.

[18] I.C. Sinka, et al., Measurement of density variations in tablets using X-ray computed tomography, Int. J. Pharm. 271 (1) (2004) 215–224.

[19] X. Jia, R.A. Williams, From microstructures of tablets and granules to their dissolution behaviour, Dissolution Technol. 13 (2) (2006) 11.

[20] G.G. Bellido, et al., The bubble size distribution in wheat flour dough, Food Res. Int. 39 (10) (2006) 1058–1066.

[21] F. Koksel, et al., The bubble size distribution and its evolution in non-yeasted wheat flour doughs investigated by synchrotron X-ray microtomography, Food Res. Int. 80 (2016) 12–18.

[22] J. Friedrich, et al., Characterization of particle size standard NIST 1019b with SynchrotronX-ray microtomography and digital data extraction, Part. Part. Syst. Charact. 29 (2012) 35–42.

[23] X. Fu, et al., Investigation of particle packing in model pharmaceutical powders using X-ray microtomography and discrete element method, Powder Technol. 167 (3) (2006) 134–140.

[24] X. Fu, et al., Application of X-ray microtomography and image processing to the investigation of a compacted granular system, Part. Part. Syst. Charact. 23 (3–4) (2006) 229–236.

[25] C.-Y. Yang, X.-Y. Fu, Development and validation of a material-labeling method for powder process characterization using X-ray computed tomography, Powder Technol. 146 (1) (2004) 10–19.

[26] J.T. Fell, J.M. Newton, Determination of tablet strength by the diametral-compression test, J. Pharm. Sci. 59 (5) (1970) 688–691.

[27] J. Berggren, G. Alderborn, Effect of drying rate on porosity and tabletting behaviour of cellulose pellets, Int. J. Pharm. 227 (1) (2001) 81–96.

[28] R.N. Elsergany, L.W. Chan, P.W.S. Heng, Influence of the porosity of cushioning excipients on the compaction of coated multi-particulates, Eur. J. Pharm. Biopharm. 152 (2020) 218–228.

[29] R.W. Heckel, Density-pressure relationships in powder compression, Trans. Metal. Soc. AIME 221 (1961) 671–675.

[30] J.A. Hersey, J. Rees, The effect of particle size on the consolidation of powders during compaction, Particle Size Analysis (1970) 33–41.

[31] R. Benabbas, et al., Performance evaluation of a novel biosourced co-processed excipient in direct compression and drug release, Polymers 13 (6) (2021) 988.

[32] E. Walker, The properties of powders. Part VI. The compressibility of powders, Trans. Faraday Soc. 19 (July) (1923) 73–82.

[33] N. Tarlier, et al., Deformation behavior of crystallized mannitol during compression using a rotary tablet press simulator, Int. J. Pharm. 547 (1) (2018) 142–149.

[34] J.M. Sonnergaard, A critical evaluation of the Heckel equation, Int. J. Pharm. 193 (1) (1999) 63–71.

[35] S. Nezamabadi, et al., Modelling the compaction of plastic particle packings, Computational Particle Mech. (2021) 1–8.

[36] M. van Hecke, Jamming of soft particles: geometry, mechanics, scaling and isostaticity, J. Phys. Condens. Matter 22 (3) (2010) 0953–8984.

[37] M. Konret, J. Vanderberghe, Comparison of laser grain size analysis with pipette and sieve analysis: a solution for the underestimation of the clay fraction, Sedimentology 44 (3) (1997) 523–535.

[38] S.J. Blott, K. Pye, GRADISTAT: a grain size distribution and statistics package for the analysis of unconsolidated sediments, Earth Surf. Process. Landf. 26 (11) (2001) 1237–1248.

[39] G. Eshel, et al., Critical evaluation of the use of laser diffraction for particle-size distribution analysis, Soil Sci. Soc. Am. J. 68 (3) (2004) 736–743.

[40] J.G. Rodríguez, A. Uriarte, Laser diffraction and dry-sieving grain size analyses undertaken on fine- and medium-grained Sandy Marine sediments: a note, J. Coast. Res. 25 (1 (251)) (2009) 257–264.

[41] M. Jonasz, Size, shape, composition, and structure of microparticles from light scattering, in: J.P.M. Syvitski (Ed.), Principles, Methods and Application of Particle Size Analysis, Cambridge University Press, Cambridge 1991, pp. 143–162.

[43] Bruker, CTan manual, Morphometric Parameters in ct-analyser, Skyscan, 2009.

[44] G.E. Reier, R.F. Shangraw, Microcrystalline cellulose in tableting, J. Pharm. Sci. 55 (5) (1966) 510–514.

[45] K.M. Picker, The use of carrageenan in mixture with microcrystalline cellulose and its functionality for making tablets, Eur. J. Pharm. Biopharm. 48 (1) (1999) 27–36.

[46] G. Thoorens, et al., Microcrystalline cellulose, a direct compression binder in a quality by design environment—a review, Int. J. Pharm. 473 (1) (2014) 64–72.

[47] J.B. Schwartz, N.H. Nguyen, R.L. Schnaare, Compaction studies on beads: compression and consolidation parameters, Drug Dev. Ind. Pharm. 20 (20) (1994) 3105–3129.

[48] S. Westermarck, et al., Microcrystalline cellulose and its microstructure in pharmaceutical processing, Eur. J. Pharm. Biopharm. 48 (3) (1999) 199–206.

[49] S.I.F. Badawy, D.B. Gray, M.A. Hussain, A study on the effect of wet granulation on microcrystalline cellulose particle structure and performance, Pharm. Res. 23 (3) (2006) 634–640.

[50] J. Staniforth, M. Chatrath, Towards a new class of high functionality tablet binders. I: quasi-hornification of microcrystalline cellulose and loss of functionality, Pharm. Res. 13 (9) (1996) S208.

[51] L. Maganti, M. Çelik, Compaction studies on pellets I. Uncoated pellets, Int. J. Pharm. 95 (1) (1993) 29–42.

[52] L. Maganti, M. Çelik, Compaction studies on pellets: II. Coated pellets, Int. J. Pharm. 103 (1) (1994) 55–67.

[53] A.-S. Persson, et al., Compression analysis for assessment of pellet plasticity: identification of reactant pores and comparison between Heckel, Kawakita, and Adams equations, Chem. Eng. Res. Des. 110 (2016).

[54] S. Patel, A.M. Kaushal, A.K. Bansal, Mechanistic investigation on pressure dependency of Heckel parameter, Int. J. Pharm. 389 (1) (2010) 66–73.

[55] N.A.K. Du Hyung Choi, et al., Material properties and compressibility using Heckel and Kawakita equation with commonly used pharmaceutical excipients, J. Pharm. Invest. 40 (4) (2010) 237–244.

[56] A.L. Skelbæk-Pedersen, et al., Investigation of the effects of particle size on fragmentation during tableting, Int. J. Pharm. 576 (2020), 118985.

[57] R.J. Roberts, Particulate analysis – mechanical properties, Solid State Characterization of Pharmaceuticals 2011, pp. 357–386.

[58] I. Ilić, et al., Deformation properties of pharmaceutical excipients determined using an in-die and out-die method, Int. J. Pharm. 446 (1–2) (2013) 6–15.

[59] D. Hooper, et al., A modern approach to the Heckel equation: the effect of CompactionPressure on the yield pressure of ibuprofen and its sodium salt, J. Nanomed. Nanotechnol. 7 (2016) 1–6.

[60] A.B. Bashaiwoldu, F. Podczeck, J.M. Newton, A study on the effect of drying techniques on the mechanical properties of pellets and compacted pellets, Eur. J. Pharm. Sci. 21 (2) (2004) 119–129.

[61] S. Patel, et al., Controlled-release domperidone pellets compressed into fast disintegrating tablets forming a multiple-unit pellet system (MUPS), J. Drug Delivery Sci. Technol. 45 (2018) 220–229.

[62] N. Tarlier, et al., Compaction behavior and deformation mechanism of directly compressible textured mannitol in a rotary tablet press simulator, Int. J. Pharm. 495 (1) (2015) 410–419.